Thermal Behavior of Composite Bridges—Insulated and Uninsulated

WILLIAM ZUK
Professor of Civil Engineering, University of Virginia, and Consultant to the Virginia Council of Highway Investigation and Research

Reported are theories and experimental data pertaining to various thermal aspects of composite bridge structures with steel beams and concrete decks or prestressed concrete beams and concrete decks, some of which are insulated on the underside with urethane foam. Heat conduction behavior as well as induced thermoelastic stresses and deformations are discussed in regard to these bridge types. Certain limited conclusions are drawn as affecting current design procedures.

•ALTHOUGH CURRENT bridge specifications in the United States, such as those of AASHO, do recognize the existence of thermal expansion and thermal forces, they are rather vague concerning values, particularly in regard to internally induced thermal stresses. Even though a bridge may have adequate provision for overall expansion and contraction, there could still exist large internal stresses due to non-uniformity in temperatures and material properties. Such is particularly true in composite structures exposed to solar radiation. German engineers and specifications were perhaps the first to deal with this subject. However, studies are now under way not only in the United States but also in Canada, England, Japan and Israel.

This paper is limited primarily to research efforts at the Virginia Council of Highway Investigation and Research located at the University of Virginia in Charlottesville. Although extensive field data have been taken in connection with this study, principal emphasis in the report is given the basic theoretical equations predicting bridge temperatures and stresses due to atmospheric weather conditions. These equations provide the greatest generality of application and are not necessarily restricted to the local conditions tested. However, as far as field conditions permit, the experimental data are compared to the theoretical to ascertain the general validity of such theories.

UNINSULATED BRIDGES

Theory of Temperature Distribution

Of first concern is the prediction of temperatures at the surface of a bridge deck. E. S. Barber (1) has developed a reasonably reliable equation to predict maximum surface temperatures of slabs, either concrete or bitumen. Although many complex factors such as solar radiation, ambient air temperature, wind velocity, insolation, reradiation, conductivity, diffusivity, and evaporation come into play, a simple but reasonable solution can be obtained on the basis of assuming average values of the secondary parameters and by assuming a sinusoidal effective daily temperature cycle.

Thus, for a normal concrete deck in the Middle Atlantic States, the maximum surface temperature in degrees Fahrenheit may be approximated by the formula

$$T_m = T_a + 0.018L + 0.667(0.50T_r + 0.054L) \quad (1a)$$

Paper sponsored by Committee on Bridges.

where

T_a = average daily air temperature (°F),
T_r = daily range in air temperature (°F), and
L = solar radiation received on a horizontal surface (cal/sq cm/day).

The equation for the maximum surface temperature of a bridge deck surfaced with a thin topping of bitumen would correspondingly be

$$T_m = T_a + 0.027L + 0.65(0.50T_r + 0.081L) \quad (1b)$$

For other regions and extreme conditions, the various constants may be appropriately adjusted as shown by Barber (1). The value of L (langleys of solar radiation) may be either determined from U. S. Weather Bureau maps or taken independently by a relatively inexpensive pyrheliometer which can be purchased commercially.

The effect of blacktopping can easily raise the surface temperature of decks 15 F or more above that of bare concrete decks. This factor is significant in relation to differential temperatures between the top and bottom of bridges, which in turn affect the induced internal thermal stresses.

The exact determination of the maximum differential temperature between the top of the slab and bottom of the supporting beam is also a complex matter. However, again with some simplifying assumptions, a rather simple but workable formula can be devised. In the case of steel beams, it is not too unreasonable to assume that the conduction of the steel is large enough that the lower outer fibers of the steel are at essentially the same temperature as the ambient air. However, there is a phase lag of several hours between the peak surface temperature (controlled primarily by solar radiation) and the air temperature, with the surface temperature generally leading the air temperature.

A simplified equation for predicting the maximum temperature differential between the top and bottom of a normal steel-concrete composite highway bridge may be assumed as

$$\Delta T_m = T_m - T_a \lambda T_r \quad (2)$$

where λ is the lag factor, varying from about one-fourth in the summer to about one-half in the winter. A value of three-eighths may be taken as an average for approximate analysis in Middle Atlantic States latitudes.

One other feature of interest is the character of the temperature distribution through the thickness of the deck slab itself. If the temperature at the top of the slab is equal to $T_t = B + C \sin(0.262t - \phi)$ and that at the bottom of the slab is $T_b = G + H \sin(0.262t)$, by superimposing the steady-state heat transfer solutions developed by Carslaw and Jaeger for periodic temperature states on an infinite plate (2), the following equation is obtained for the time-temperature-depth relation:

$$T = CY \sin(0.262t - \phi + \ln Y) + HY' \sin(0.262t) + (B-G)\frac{y}{h} + G \quad (3)$$

where

h = thickness of slab,
y = distance measured from bottom of slab,
t = time,

$$Y = \left[\frac{\cosh 2my - \cos 2my}{\cosh 2mh - \cos 2mh}\right]^{1/2}, \text{ and}$$

$$Y' = \left[\frac{\cosh 2m(h-y) - \cos 2m(h-y)}{\cosh 2mh - \cos 2mh}\right]^{1/2}.$$

In the last two terms, $m = \left(\frac{0.262}{2q}\right)^{1/2}$ where q is the diffusivity (an approximate value of m for concrete is 2.1 in units of feet, hours, pounds, British thermal units, and degrees Fahrenheit).

Generally speaking, in normal bridge structures, a temperature extreme (either hot or cold) at the top of the slab rapidly decays with depth, so that at approximately mid-depth the temperature is virtually the same as at the bottom of the slab.

Theory of Thermoelastic Stresses and Deformation—Composite Section with Steel Beam and Concrete Deck

The following theory follows in essence the derivations in a previous paper (3), except for the consideration of temperature varying as any function of depth instead of a linear function. The theory in this paper, therefore, represents a more generalized case. The slab and beam are assumed separated and free to deform independently according to the imposed temperature conditions. From basic thermoelastic theory, these separated induced thermal stresses may be easily determined. From these stresses, acting in conjunction with thermal expansion, the strains at any depth of the beam or slab may be found. However, in the actual composite beam, additional unknown forces in the nature of shears and couples exist at the interface between the slab and beam at the ends (3). These interface forces cause the two separated elements to join compositely, so that the strain of both the beam and the slab at the interface must be equal (assuming a no-slip condition) and the radius of curvature at the interface must be the same for the slab and the beam.

When the strain effects of the interface shears and couples are superimposed with the original thermal strains and the compatibility conditions of equal strain and curvature at the interface are met, the values of the interface shear and moment may be determined. Once these are established, the actual stresses and deformations in the composite section may be found by elementary beam theory.

Notations.—The symbols used in the following derivation are defined as follows:

- A = cross-sectional area of beam,
- a = half of depth of slab,
- $b(y)$ = width of beam at various depths,
- E_c = modulus of elasticity of concrete,
- E_b = modulus of elasticity of steel beam,
- ϵ_b = induced unit strain in beam,
- ϵ_s = induced unit strain in slab,
- F = interface shear force,
- f_b = induced stress in beam,
- f_s = induced stress in slab,
- I = moment of inertia of beam section,
- D = beam span,
- μ = Poisson's ratio,
- p = width of slab,
- Q = interface couple,
- ν = vertical deflection of beam at midspan,
- α_c = coefficient of thermal expansion of concrete,
- α_b = coefficient of thermal expansion of steel beam,
- T = temperature, and
- T_o = initial temperature.

Derivation.—From elastic theory, the general thermal stress-strain equations are as follows:

$$\epsilon_x = \frac{1}{E}\left[f_x - \mu(f_y + f_z)\right] + \alpha \Delta T$$

$$\epsilon_y = \frac{1}{E}\left[f_y - \mu(f_z + f_x)\right] + \alpha \Delta T$$

$$\epsilon_z = \frac{1}{E}\left[f_z - \mu(f_x + f_y)\right] + \alpha \Delta T \qquad (4)$$

Referring to Figure 1 using a (x_1, y_1, z_1, T_1) coordinate system for the slab and considering the slab restrained in the z_1 direction ($\epsilon_{z_1} = 0$) by adjacent beams and free in the y_1 direction, one may derive from Eq. 1 the following relations for slab stresses:

$$f_{z_1 s} = \mu f_{x_1 s} - \alpha_c E_c \left[T_1(y_1) - T_o\right]$$

and

$$f_{y_1 s} = 0 \qquad (5)$$

When the slab is assumed to be separated from the beam but subjected to the actual temperature distribution $T_1(y_1)$, the following general equation may be used to determine $f_{x_1 s}$ in the slab (3):

$$f_{x_1 s} = \frac{\alpha_c E_c\left[T_1(y_1) - T_o\right]}{1-\mu} + \frac{\alpha_c E_c}{2a(1-\mu)} \int_{-a}^{+a} \left[T_1(y_1) - T_o\right] dy +$$

$$\frac{3\alpha_c E_c y_1}{2a^3(1-\mu)} \int_{-a}^{+a} \left[T_1(y_1) - T_o\right] y_1 \, dy_1 \qquad (6)$$

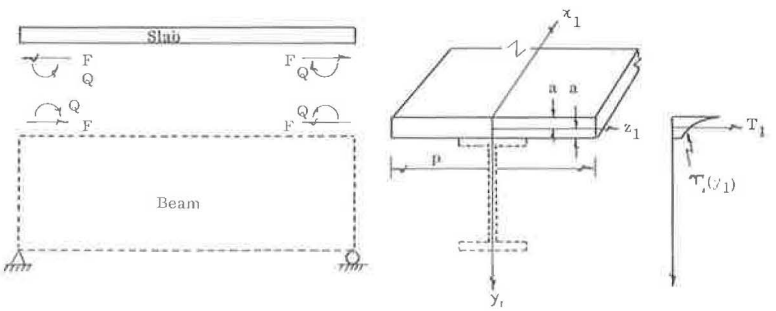

Figure 1.

The corresponding strain $\epsilon_{x_1 s}$ may be found from Eq. 4 as:

$$\epsilon_{x_1 s} = \frac{1}{E_c} \left[f_{x_1 s} - \mu f_{z_1 s} \right] + \alpha_c \left[T_1(y_1) - T_o \right] \tag{7}$$

Substituting Eq. 5 and 6 in Eq. 7, one may obtain the following expression to determine $\epsilon_{x_1 s}$ in the slab.

$$\epsilon_{x_1 s} = \frac{(1 + \mu)\,\alpha_c}{2a} \int_{-a}^{+a} \left[T_1(y_1) - T_o \right] dy_1 + \frac{3(1 + \mu)\,\alpha_c\, y_1}{2a^3} \int_{-a}^{+a} \left[T_1(y_1) - T_o \right] y_1\, dy_1 \tag{8}$$

at $y_1 = 0$, making,

$$\epsilon_{x_1 s} = \frac{(1 + \mu)}{2a} \int_{-a}^{+a} \left[T_1(y_1) - T_o \right] dy_1 \tag{9}$$

and at $y_1 = a$,

$$\epsilon_{x_1 s} = \frac{(1 + \mu)\,\alpha_c}{2a} \int_{-a}^{+a} \left[T_1(y_1) - T_o \right] dy_1 + \frac{3(1 + \mu)\,\alpha_c}{2a^2} \int_{-a}^{+a} \left[T_1(y_1) - T_o \right] y_1\, dy_1 \tag{10}$$

The bottom slab strain (at $y_1 = a$) due to the interface shears and moments is

$$\epsilon'_{x_1 s} = \frac{(1 - \mu^2)}{ap\,E_c} \quad \frac{3Q}{2F - 2a} \tag{11}$$

Thus, the sum of Eqs. 10 and 11 gives the total interface strain of the slab:

$$\epsilon''_{x_1 s} = \frac{(1 - \mu^2)}{ap\,E_c} \quad 2F - \frac{3Q}{2a} + \frac{(1 + \mu)\,\alpha_c}{2a} \int_{-a}^{+a} \left[T_1(y_1) - T_o\right] dy_1 +$$

$$\frac{3(1 + \mu)\,\alpha_c}{2a^2} \int_{-a}^{+a} \left[T_1(y_1) - T_o\right] y_1\, dy_1 \tag{12}$$

Considering the beam separated from the slab, using a (x_1, y_1, z_1, T) coordinate system as shown in Figure 2, the following equation may be used to determine f_{xb} in the beam section due to the temperature change (3):

$$f_{xb} = \alpha_b E_b \left[T(y) - T_o\right] + \frac{\alpha_b E_b}{A} \int_{-d_1}^{+d_2} \left[T(y) - T_o\right] b(y)\, dy +$$

$$\frac{\alpha_b E_b y}{I^2} \int_{-d_1}^{+d_2} \left[T(y) - T_o\right] b(y)\, y\, dy \tag{13}$$

Since the beam is free in both y and z directions ($f_{yb} = f_{zb} = 0$), one may derive from Eq. 4 the following stress-strain relation for the beam:

$$\epsilon_{xb} = \frac{f_{xb}}{E_c} + \alpha_b \left[T(y) - T_o\right] \tag{14}$$

Substituting Eq. 13 into Eq. 14, one may obtain the corresponding strain as

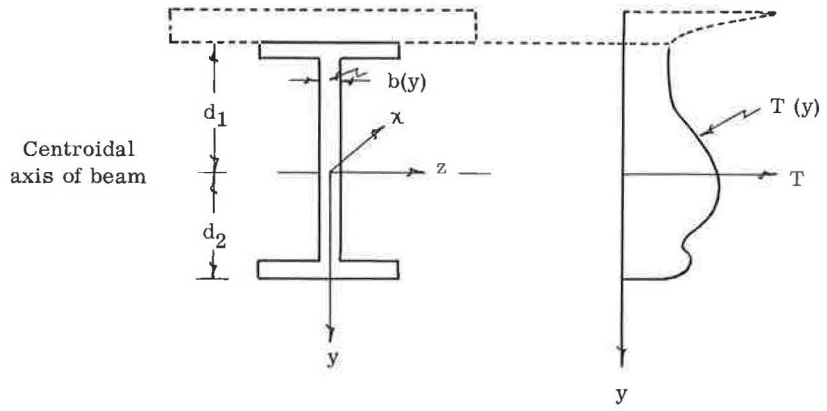

Figure 2.

$$\epsilon_{xb} = \frac{\alpha_b}{A}\int_{-d_1}^{+d_2}\left[T(y) - T_o\right] b(y)\,dy + \frac{\alpha_b y}{I}\int_{-d_1}^{+d_2}\left[T(y) - T_o\right] b(y)\,y\,dy \qquad (15)$$

making, at $y = d_1$,

$$\epsilon_{xb} = \frac{\alpha_b}{A}\int_{-d_1}^{+d_2}\left[T(y) - T_o\right] b(y)\,dy - \frac{d_1\alpha_b}{I}\int_{-d_1}^{+d_2}\left[T(y) - T_o\right] d(y)\,y\,dy \qquad (16)$$

The stress and strain in the beam caused by the interface forces are

$$f_{xb'} = \frac{Qy}{I} + F\left(\frac{d_1 y}{I} - \frac{1}{A}\right) \qquad (17)$$

$$\epsilon_{xb'} = \frac{Qy}{IE_b} + \frac{F}{E_b}\left(\frac{d_1 y}{I} - \frac{1}{A}\right) \qquad (18)$$

and at $y = -d_1$,

$$\epsilon_{xb'} = -\frac{Qd_1}{IE_b} - \frac{F}{E_b}\left(\frac{d_1^2}{I} + \frac{1}{A}\right) \qquad (19)$$

Therefore, the sum of Eqs. 16 and 19 gives the total interface strain of the beam at $y = -d_1$ as follows:

$$\epsilon''_{xb} = -\frac{Qd_1}{IE_b} - \frac{F}{E_b}\left(\frac{d_1^2}{I} + \frac{1}{A}\right) + \frac{\alpha_b}{A}\int_{-d_1}^{+d_2}\left[T(y) - T_o\right] b(y)\,dy - \frac{d_1\alpha_b}{I}\int_{-d_1}^{+d_2}\left[T(y) - T_o\right] b(y)\,y\,dy \quad (20)$$

For compatibility of horizontal strains between slab and beam at the interface, Eq. 12 must equal Eq. 20, which gives

$$\left[\frac{1}{AE_b} + \frac{d_1^2}{IE_b} + \frac{2(1-\mu^2)}{apEc}\right]F + \left[\frac{d_1}{IE_b} - \frac{3(1-\mu^2)}{2a^2 pEc}\right]Q = -\frac{(1+\mu)\alpha_c}{2a}\left\{\int_{-a}^{+a}\left[T_1(y_1) - T_o\right]dy_1 + \frac{3}{a}\int_{-a}^{+a}\left[T_1(y_1) - T_o\right]y_1\,dy_1\right\} + \alpha_b\left\{\frac{1}{A}\int_{-d_1}^{+d_2}\left[T(y) - T_o\right]b(y)\,dy - \frac{d_1}{I}\int_{-d_1}^{+d_2}\left[T(y) - T_o\right]b(y)\,y\,dy\right\} \quad (21)$$

Subtracting Eq. 9 from Eq. 10, one may obtain the strain difference between the midplane and bottom of slab induced by temperature change in the concrete section:

$$\epsilon_{x_1 s} \text{ (difference)} = \frac{3(1+\mu)\alpha_c}{2a^2} \int_{-a}^{+a} \left[T(y) - T_o\right] y\,dy \tag{22}$$

The strain difference induced by the interface forces as the same positions is given by:

$$\epsilon_{x_1 s'} \text{ (difference)} = \frac{3(1-\mu^2)}{2a^2\, pE_c} (Fa - Q) \tag{23}$$

Therefore, the total strain differential is the sum of Eqs. 22 and 23:

$$\epsilon_{x_1 s} \text{ (total difference)} = \frac{3(1-\mu^2)}{2a^2\, pE_c} (Fa - Q) + \frac{3(1+\mu)\alpha_c}{2a^2} \int_{-a}^{+a} \left[T_1(y_1) - T_o\right] y_1\,dy_1 \tag{24}$$

This differential strain may then be related to the radius of curvature of the slab at the interface by simple geometry as follows:

$$R_s = \frac{2a^3\, p\, E_c}{3(1-\mu^2)(Fa - Q) + 3(1+\mu)\, p\alpha_c\, E_c \int_{-a}^{+a} \left[T_1(y_1) - T_o\right] y_1\,dy_1} + a \tag{25}$$

Considering the beam alone, the total induced moment is

$$M_t = Fd_1 + Q + \alpha_b E_b \int_{-d_1}^{+d_2} \left[T(y) - T_o\right] b(y)\, y\, dy \tag{26}$$

The radius of curvature of the beam at the interface may be found by elementary flexure theory:

$$R_b = \frac{E_b I}{Fd_1 + Q + \alpha_b E_b \int_{-d_1}^{+d_2} \left[T(y) - T_o\right] b(y)\, y\, dy} - d_1 \tag{27}$$

The second term in both Eqs. 25 and 27 is so small in comparison to the first term that it can be omitted without introducing significant error. Thus, the vertical compatibility is written by equating Eqs. 25 and 27, which may be rearranged as follows:

$$\left[2pd_1 a^3 E_c - 3(1 - \mu^2) aIE_b\right] F + \left[2pa^3 E_c + 3(1 - \mu^2) IE_b\right] Q =$$

$$3(1 + \mu)\, p\alpha_c IE_b E_c \int_{-a}^{+a} \left[T_1(y_1) - T_o\right] y_1\, dy_1 -$$

$$2pa^3 \alpha_b E_b E_c \int_{-d_1}^{+d_2} \left[T(y) - T_o\right] b(y)\, y\, dy \tag{28}$$

The unknown quantities F and Q may be obtained by solving Eqs. 21 and 28 simultaneously. For practical purposes, these equations are best solved numerically for particular problems.

With F and Q known, the stress $f_{x_1 s}$ in the slab is obtained by adding Eq. 6 to the stresses induced by the interface forces, giving:

$$f_{x_1 s} = \frac{F}{2ap} + \frac{3(Fa - Q) y_1}{2a^3 p} - \frac{\alpha_c E_c \left[T_1(y_1) - T_o\right]}{1 - \mu} +$$

$$\frac{\alpha_c E_c}{\mu} \int_{-a}^{+a} \left[T_1(y_1) - T_o\right] dy_1 + \frac{3\alpha_c E_c y_1}{\mu} \int_{-a}^{+a} \left[T_1(y_1) - T_o\right] y_1\, dy_1 \tag{29}$$

Similarly, the stress f_{xb} in the beam is the sum of Eqs. 13 and 17. The stress in the slab in the transverse or z_1 direction is obtained from Eq. 5.

The induced moment in Eq. 26 causes a deflection of the beam which may be obtained from the elementary equation of flexure of a simply supported beam acted on by a constant moment:

$$\nu_{max} = \frac{Q^2}{8 E_b I} \left\{ F d_1 + Q + \alpha_b E_b \int_{-d_1}^{+d_2} \left[T(y) - T_o \right] b(y)\, y\, dy \right\} \tag{30}$$

Composite Section with Precast-Prestressed Concrete Beam and Concrete Deck

The detailed theory involved in this case is presented in a recent paper (4). In broad outline, the approach is similar to that explained in the steel-concrete composite section, except for the added stress and strain effects of the prestressing tendon. Although two cases of prestressing tendons were studied, one involving a straight tendon and the other involving a parabolically draped tendon, for brevity only the summary equations for the straight tendon are presented in this report. The pertinent equations are as follows:

$$\left(\frac{1}{AE_c} + \frac{1}{A_t E_t} + \frac{e^2}{IE_c} \right) F_t - \frac{e}{IE_c} Q + \frac{1}{E_c} \left(\frac{1}{A} - \frac{e d_1}{I} \right) F =$$

$$- \alpha_t \left[T(e) - T_o \right] + \frac{\alpha_c}{A} \int_{-d_1}^{+d_2} \left[T(y) - T_o \right] b(y)\, dy + \frac{e \alpha_c}{I} \int_{-d_1}^{+d_2} \left[T(y) - T_o \right] b(y)\, y\, dy \tag{31}$$

$$\left(\frac{1}{A} - \frac{e d_1}{I} \right) F_t + \left[\frac{d_1}{I} - \frac{3(1 - \mu^2)}{2a^3 p} \right] Q + \left[\frac{1}{A} + \frac{d_1^2}{I} + \frac{2(1 - \mu^2)}{ap} \right] F =$$

$$\alpha_c E_c \left\{ - \frac{1 + \mu}{2a} \int_{-a}^{+a} \left[T_1(y) - T_o \right] dy_1 - \frac{3(1 + \mu)}{2a^2} \int_{-a}^{+a} \left[T_1(y_1) - T_o \right] y_1\, dy_1 + \right.$$

$$\left. \frac{1}{A} \int_{-d_1}^{+d_2} \left[T(y) - T_o \right] b(y)\, dy - \frac{d_1}{I} \int_{-d_1}^{+d_2} \left[T(y) - T_o \right] b(y)\, y\, dy \right\} \tag{32}$$

and

$$2a^3 pe F_t - \left[2a^3 p + 31(1-\mu^2)\right] Q + \left[3aI(1-\mu^2) - 2a^3 pd_1\right] F =$$

$$p\alpha_c E_c \left\{ -3(1+\mu) I \int_{-a}^{+a} \left[T_1(y_1) - T_o\right] y_1 dy_1 + 2a^3 \int_{-d_1}^{+d_2} \left[T(y) - T_o\right] b(y)\, y dy \right\} \quad (33)$$

where e is the distance of the tendon from the centroidal axis of the beam, and the subscript t refers to the tendon.

Eqs. 31, 32, and 33 are solved simultaneously (best done numerically) for the factors F, Q, and F_t, where F_t is the change in prestressing force due to the temperature effects. The corresponding slab stresses are found by use of Eqs. 5 and 29.

The beam stresses are found as follows:

$$f_{xb} = F_t \left(\frac{1}{a} + \frac{ey}{I}\right) + \frac{Qy}{I} + F\left(\frac{d_1 y}{I} - \frac{1}{A}\right) - \alpha_c E_c \left[T(y) - T_o\right] +$$

$$\frac{\alpha_c E_c}{A} \int_{-d_1}^{+d_2} \left[T(y) - T_o\right] b(y)\, dy + \frac{\alpha_c E_c y}{I} \int_{-d_1}^{+d_2} \left[T(y) - T_o\right] b(y)\, y dy \quad (34)$$

The maximum vertical deflection at the center of this simply supported prestressed beam due to the temperature is

$$\nu_{max} = \frac{D^2}{8 E_c I} \left\{ Fd_1 + Q - F_t e + \alpha_c E_c \int_{-d_1}^{+d_2} \left[T(y) - T_o\right] b(y)\, y dy \right\} \quad (35)$$

Field Tests

To obtain data on actual field conditions of temperature and thermal strains on a bridge, a composite steel girder and concrete slab bridge over the Hardware River near Charlottesville was instrumented (Fig. 3).

Twenty-two iron-constantan thermocouples were embedded near the top of the slab, at the mid-depth of slab, at the top of the steel beams, at the mid-depth of the beam,

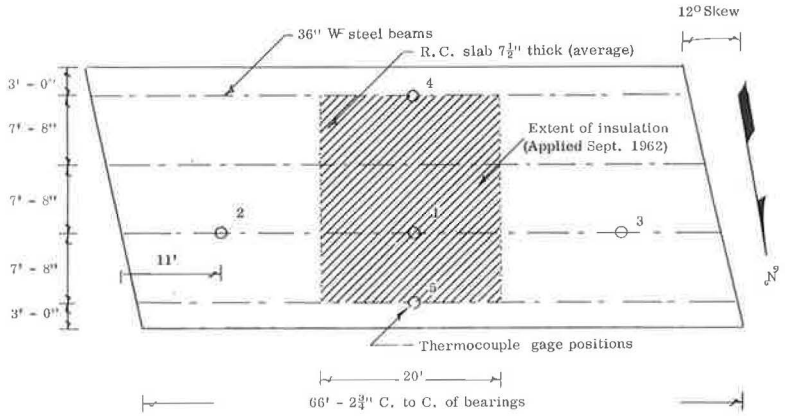

Figure 3. Plan of bridge.

and at the bottom of the beam at the positions shown in Figure 3. Two ambient air temperature gages were also installed at Positions 2 and 3. The thermocouples were all wired to a Minneapolis-Honeywell 24-point recorder which scanned and recorded all the points automatically once an hour.

Periodic strain readings were taken manually in the beam and slab at Position 1 by a 10-in. Whittemore strain gage, compensated by an invarient invar bar. A mechanical device instead of an automatic electrical device was selected for strain readings to insure greater long-term reliability. To isolate the temperature-induced strains, readings were taken only under dead load and constant moisture conditions in the slab. Slab moisture was detected by a nuclear moisture probe using a radium-beryllium source manufactured by Nuclear-Chicago.

When the testing was initiated, the bridge structure was 2 years old, so essentially all shrinkage had already taken place. Rod and level readings were taken at the same time strains were measured. All data were thus read and recorded for the period from September 1961 to August 1962, with the exception of June and July because of persistent instrument malfunctions. However, from September 1962 to May 1963 only temperature data were recorded (for reasons to be discussed later). As it is obviously impractical to present all accumulated data, only those believed to be meaningful or typical are presented.

The extreme low temperature, -6 F, was recorded in January 1962 from midnight to 6 A.M. at the bottom of the steel flanges. The air temperature at this time was also -6 F. The highest temperature recorded, 123 F, was in May 1963 at 3 P.M. at the top of the slab. The air temperature at this time was 97 F.

The maximum temperature differential through the depth of the bridge at an interior beam at any given time did not exceed 37 F, when the slab was warm and the beam was cool. This situation typically occurred during sunny afternoons when the sun's radiations coupled with high air temperatures warmed the top of the slab. Oddly enough, the reverse condition prevailed on outside beams exposed to the sun. A maximum differential temperature of 42 F was observed on such an exterior beam in January on a sunny but cold afternoon. The result was that the top of the slab remained relatively cool (although warmed to some degree by the sun) while the exposed lower portion of the steel beam with its high thermal conductivity was heated. Other than for these edge beams and isolated regions shaded by railings or trees, the temperature at any given strata of the bridge was practically constant.

Since it is the temperature gradient that contributed to high internal thermal stresses, high thermal differentials are most important. Large temperature fluctuations from winter to summer, although causing large overall expansion or contraction, do not normally play a large role in internal stresses.

As an adjunct experiment, temperature readings were taken at the surface of normal grey-white concrete and black-grey bituminous concrete. Due to color, the darker surface absorbed more short-wave solar radiation, raising the bituminous temperature approximately 15 F higher than that of the normal concrete on a sunny summer afternoon. On a sunny winter afternoon, only a 5 F differential was noted.

These experimental data correlate well with the theory presented in Eqs. 1a and 1b, in which solar radiation was measured near the site with a portable Belfort recording pyrheliometer.

A typical plot of temperatures on an interior region of the bridge for a day in March 1963 is shown in Figure 4. Based on the measured solar radiation for that day, L is 471.3. Using Eq. 1a, the maximum surface temperature is 102 F, compared to the true measured value of 98 F. Similarly, the maximum differential temperature based on Eq. 2 is 24 F, compared to the true measured temperature of 23 F. On sunny days, the sun's radiation often heats the top of the deck 20 or 30 F higher than the air temperature by mid-afternoon.

To illustrate the difference in thermal behavior between an interior and an exterior beam on a cool sunny day in January 1962, the log of temperatures in Figure 5 is presented. The general trends and distributions of temperature are about the same for a warm sunny day at any season of the year. There is a continuous variation due to conductivity and radiation.

Generally speaking, for an interior beam, the lower flanges rapidly assume the surrounding air temperature due to the steel's high conductivity. The conductivity of the concrete slab is lower, with the bottom surface and especially the middle temperatures generally lagging the air temperature. As is observed, the bottom slab temperature affects the temperature at the top of the steel beam, mostly through conduction. At night the temperature gradients are generally rather small, and it is occasionally observed that the top of the slab is at a temperature a few degrees lower than that of the air due to reverse long-wave radiation from the slab to the black sky. In the early hours of the morning, the entire bridge is often at a constant temperature, that of the air. This is also true during all the daylight hours on cloudy or rainy days.

The steep thermal gradients in the slab near the upper surface are characteristic. Spot check comparisons of the experimental data with the theory (Eq. 3) show agreement of about 10 percent. The most significant source of error lies in the theoretical assumption that the boundary temperatures vary as a sine wave, whereas a glance at a typical temperature curve as in Figure 4 shows this to be only approximately true.

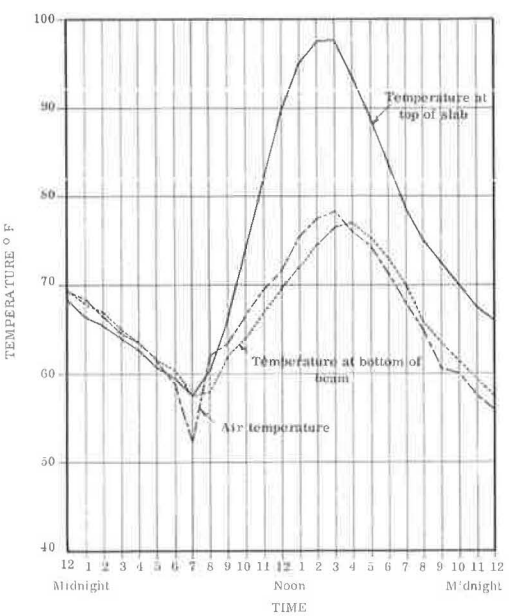

Figure 4. Plot of temperatures for March 18, 1963.

In regard to strain and deformation measurements, unexpected complications arose. Strain readings were not compared to theory until many months after the initiation of the testing program, at which time it was observed that (a) there was considerable interface slip between the steel and the concrete and (b) there were appreciable axial end restraints on the bridge at the positions of the slab and the bearing plate. The slip behavior was most erratic, precluding any easy explanation or correction. (This bridge has stud-type shear connectors.) As time progressed (particularly with the coming of warm weather) it was noticed that the entire bridge expanded to such an extent that several of the 1-in. diameter anchor bolts were bent and a 12-in. reinforced concrete

Time	Exterior Beam	Interior Beam	Air Temp. Deg. F	Time	Exterior Beam	Interior Beam	Air Temp. Deg. F
Midnight	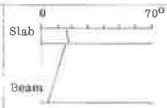	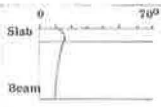	8	12:00 A.M.	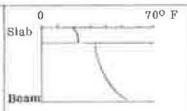	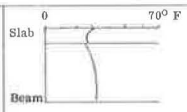	35
1:00 A.M.	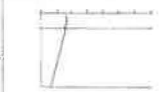	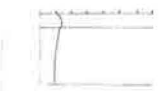	7	1:00 P.M.	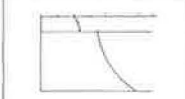	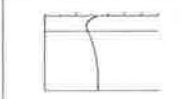	37
2:00 A.M.	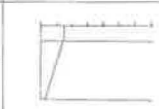	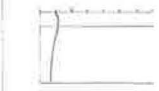	3	2:00 P.M.	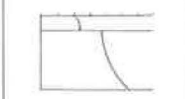	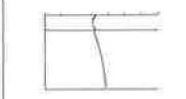	36
3:00 A.M.	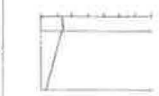	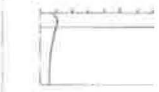	3	3:00 P.M.	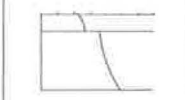	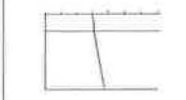	28
4:00 A.M.	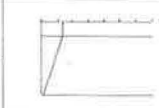	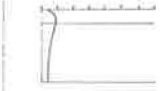	1	4:00 P.M.	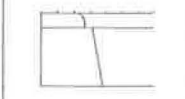	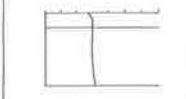	27
5:00 A.M.	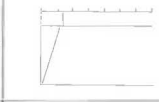	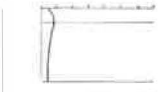	1	5:00 P.M.	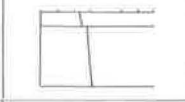	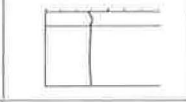	25
6:00 A.M.	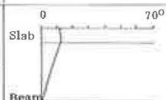	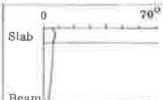	2	6:00 P.M.	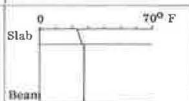	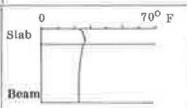	23
7:00 A.M.	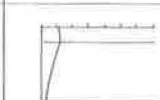	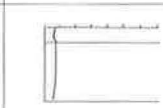	7	7:00 P.M.		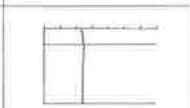	22
8:00 A.M.	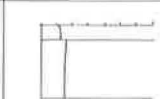		17	8:00 P.M.		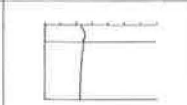	20
9:00 A.M.	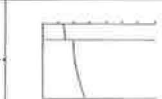	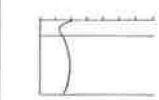	25	9:00 P.M.	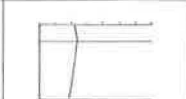	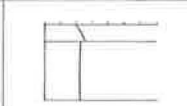	18
10:00 A.M.			28	10:00 P.M.			17
11:00 A.M.			32	11:00 P.M.			14

Figure 5. Temperature log.

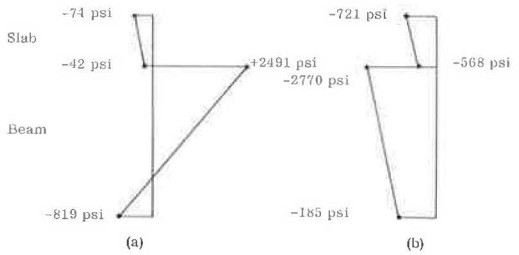

Figure 6. Stress distributions.

back wall was cracked from pressure transmitted through a 1-in. thick expansion filler at the slab level.

Because of these unexpected and unmeasured complications, attempts at reconciling the theory with experiments proved futile. As a case in point, for a temperature state with the top of the slab at 104 F and the beam and the bottom of the slab at 93 F, Figure 6a shows the theoretical stress distribution in the longitudinal direction. Figure 6b shows the actual stresses from measured strains.

To adjust these divergent results, theoretically there must exist an axial compressive stress at the end of the slab of 689 psi and a bearing force at the anchor bolts of 15,020 lb. Interface slip would tend to reduce these restraint values, but to an unknown extent as no reliable slip theory is yet available. A complete theory would also have to take into account creep and plasticity effects. For similar reasons, deformation measurements also had to be discarded.

INSULATED BRIDGES

In September 1962, a 1-in. thick coating of sprayed foam urethane insulation was applied to that portion of the Hardware River Bridge shown in Figure 3. The insulation was applied not only as is customary on the underside of the concrete deck, but also completely around the exposed portion of the supporting steel beams, including the webs and the lower flanges. As is seen in Figure 3, part of the bridge was left uninsulated for comparison.

The normal use of bridge insulation is to reduce the number of freeze-thaw cycles of the top surface of the deck and to delay or eliminate premature icing of the deck as compared to the adjacent soil-based road surface. However, the primary object of this experiment was to determine how insulation affects the induction of thermal stresses and, therefore, the full beam was coated.

Figures 7 and 8 show the comparative temperatures at the top and bottom of the bridge, insulated and uninsulated, for a cold sunny day in November 1962, with the air temperature near freezing during the early morning hours. The comparative behavior on a warm sunny day in April 1963 is shown in Figures 9 and 10. The trends on both cold and warm sunny days are the same.

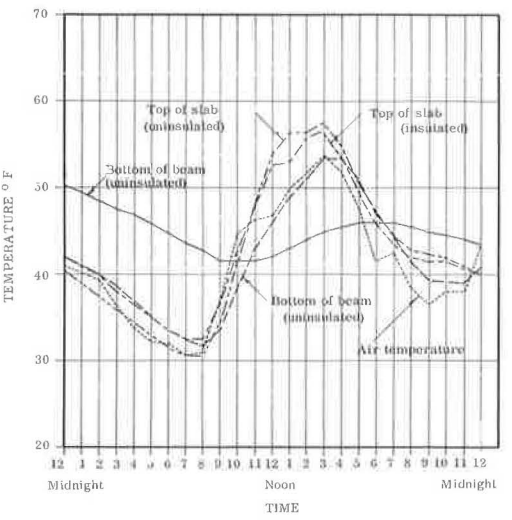

Figure 7. Plot of temperatures for November 23, 1962.

The observed data indicate that the presence of full insulation increases the maximum temperature differential between the top and bottom of the bridge by approximately 25 percent over uninsulated bridges. In building roof structures, the reverse is true (5). Although the thermodynamic theory explaining this bridge behavior quantitatively has not yet been fully worked out by the author, a qualitative explanation can be had from Figures 7 and 9. In regard to the bottom of the beam curve (insulated), the insulation serves to level out the extreme variations of the ambient air temperatures. Coupled with this, there is a time lag of many hours due to the insulating qualities around the steel. The net result is a decided increase in maximum temperature differential in the bridge oc-

Figure 8. Temperature log, Hardware River Bridge.

curring in the early afternoon. The maximum differential temperature observed in these tests was 41 F in May 1963. Such a condition, therefore, appreciably increases the maximum induced internal thermal stresses in the structure, and is thus undesirable from a stress point of view.

During the colder non-daylight hours, the top of the insulated deck is a few degrees warmer than the uninsulated deck. For atmospheric conditions just below freezing, these few degrees could indeed make the difference between an iced or a non-iced deck. During the sunny daylight hours, the slab temperature conditions are reversed, with the uninsulated slab being warmer than the insulated one. Again, a qualitative explanation serves to explain this reversal. During the night, the warm stored heat flux in the insulated lower beam flows to the cooler surface where the heat warms the surface and

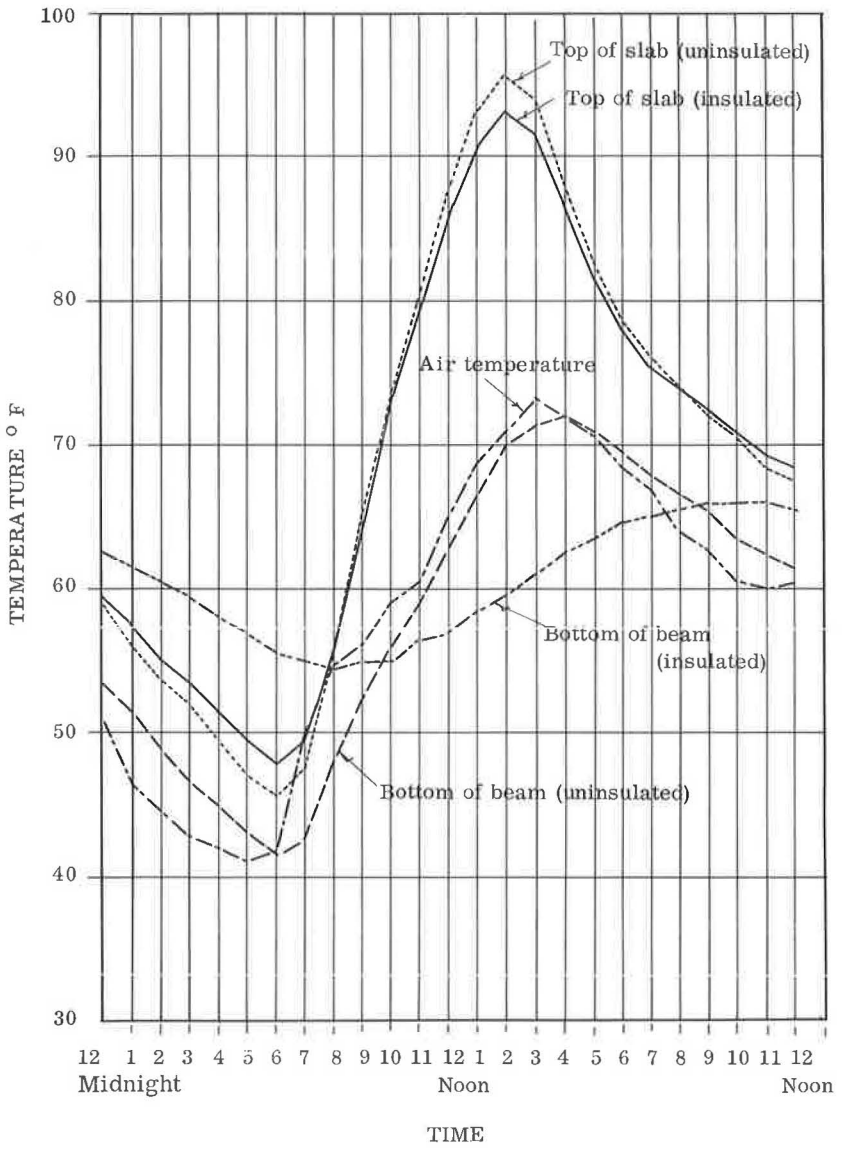

Figure 9. Plot of temperatures for April 8, 1963.

the boundary layer of air above it. However, during the day, the solar warmed boundary layer of air and the insulated slab surface are considerably hotter than the bottom of the beam, causing the heat flux to flow downward. This downward flow drains some heat energy from the surface of the slab, thereby slightly cooling it.

As a simple side experiment to test bounding characteristics, urethane foam was sprayed on test samples of bare aluminum, bare steel, and steel coated with aluminum paint. It is parenthetically noted that the insulation peeled off the aluminum in about 5 weeks, and off the bare steel in about 5 months of semi-protected outside exposure. The bond on the painted steel sample is still holding well as of this date, although some edge peeling is observed on the actual bridge.

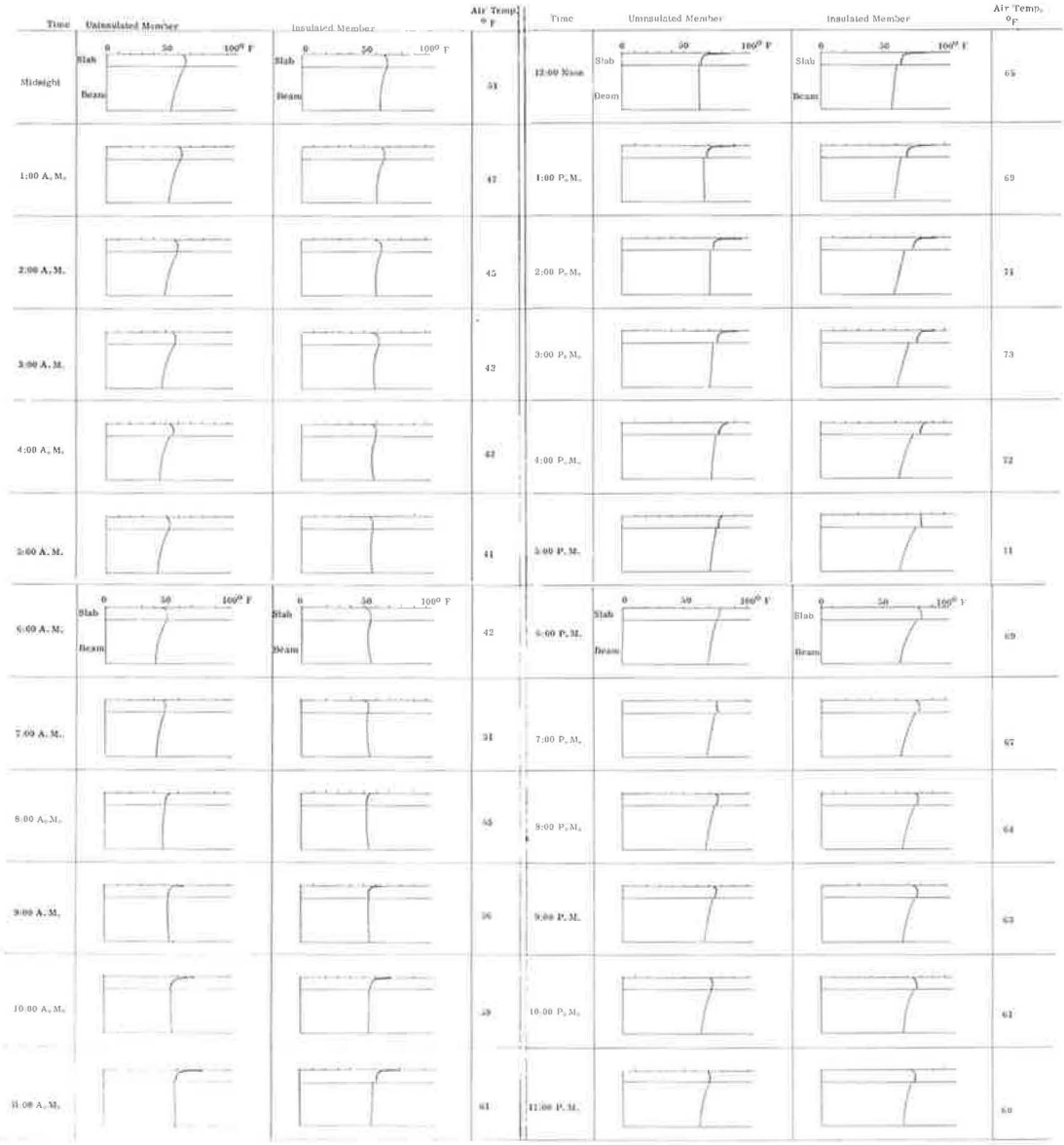

Figure 10. Temperature log, Hardware River Bridge.

EXAMPLES AND GENERAL CONCLUSIONS

It has been seen in earlier sections of this paper that the theoretical heat transfer equations have generally been supported by experiment. However, no confirmation or repudiation of the theoretical stress equations by experiment has been possible in this study. Therefore, a few typical numerical examples will be presented to obtain a "feel" for the thermoelastic stresses and deformations.

Consider a reasonable temperature distribution as shown in Figure 11a applied to the Hardware River Bridge. By use of the stress equations derived in this paper, assuming T_o = 60 F and typical material properties, the resulting longitudinal stresses, f_x, developed will appear as in Figure 11b.

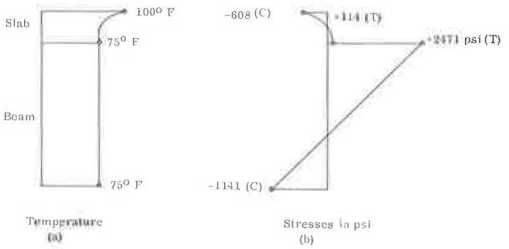

Figure 11.

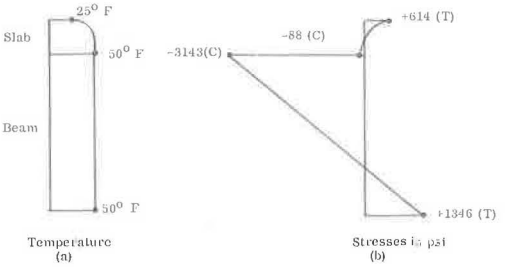

Figure 12.

The maximum transverse stress in the slab, f_{Z_1S}, will be 109.6 psi (c), and the maximum thermal deflection, ν, will be 0.26 in. up. Of equal, if not more importance, is the development of theoretical large interface shears and couples concentrated within inches of the end. In this example the shear, F, equals 32,042 lb, and the couple, Q, equals 396,861 in.-lb. Q is physically manifested by the existence of normal pressures of compression and tension acting side by side on the interface surfaces or connectors within inches of the end of the beam. Since these large forces obviously cause slip and local yielding of the material, in actuality these interface stresses must be, to some unknown degree, less than predicted. This would then be followed by a decrease in all other thermal stresses and deflections.

For the temperature distribution in Figure 11a the stresses in the beam are of reverse sign to that of dead or live loads. Consequently, they would generally not be detrimental. However, should the temperature pattern be as shown in Figure 12a, the resulting stresses in Figure 12b would be additive to the dead and live load stresses. In this second example, F = 43,273 lb, Q = 430,563 in.-lb, ν = 0.32 in. down, and the maximum f_{Z_1S} = 980 psi (T). Larger differential temperatures would obviously induce even higher stresses (although not proportionally) so that thermal differentials of 40 or 50 F could conceivably cause overstress of design allowables when coupled with dead loads, live loads and shrinkage.

Consideration too must be given to the eventuality of a concrete bridge deck being surfaced with blacktopping; this would generally increase the maximum thermal differential. Studies (5) show that a 2-in. topping is necessary before the insulating effect of the surfacing begins to offset the increase in temperature due to the darker color. Atmospheric conditions, such as air temperature, solar radiation, humidity, and wind velocity, at the time of construction also play a role in the induction of thermal stresses, complicated by complex relations of shrinkage and time-dependent changes in concrete properties during hardening.

German bridge specifications (6) do require provisions for temperature stresses in composite members. In particular, they specify for design (a) a temperature difference of ± 15 C (± 27 F) between the concrete slab and the steel beam, (b) special heavy end anchorages tieing the slab and the beam together at their interface, and (c) in the absence of more exact analysis, a distribution of end interface shear which is maximum at the end and linearly decreases to zero at a distance from the equal to the effective width of the slab. Sattler (7) has performed quantitative thermal analysis where the slab is at one uniform temperature and the beam at another uniform temperature. This condition only roughly approximates the actual nonlinear distribution of temperature considered in this paper.

An example of a prestressed-composite beam is a typical AASHO-PCI Type IV precast-prestressed beam shown in Figure 13 with a 100-ft span. Assuming a temperature distribution as shown in Figure 14a, the resulting longitudinal stresses (derived from the previous theoretical equations) are shown in Figure 14b. The initial temperature T_O is taken as 60 F. For this case, the interface shear is 19,600 lb, the interface moment is 80,300 in.-lb, the maximum transverse stress in the slab is 302 psi (c), the loss of prestress in the tendon is 0.86 percent, and the maximum center deflection is 0.36 in. down.

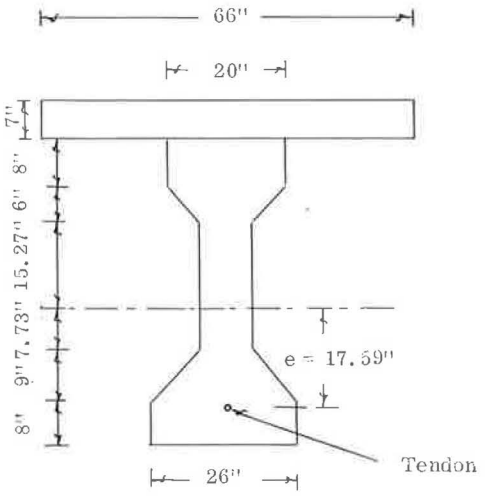

Figure 13.

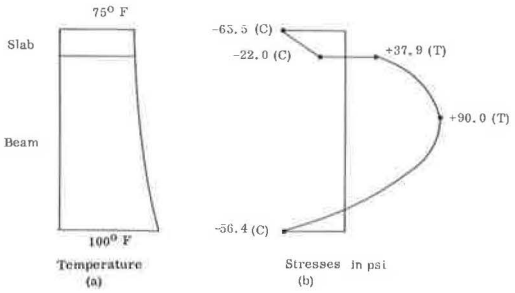

Figure 14.

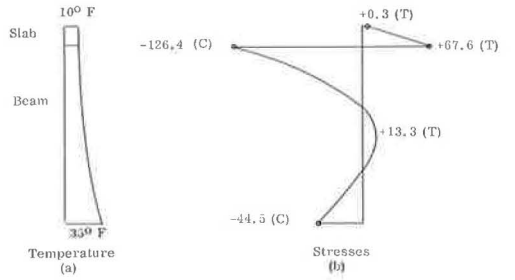

Figure 15.

For a different temperature distribution as shown in Figure 15a, the resulting longitudinal stresses are shown in Figure 15b. The interface shear is 16,290 lb, the interface moment is 38,890 in.-lb, the maximum transverse stress in the slab is 970-psi tension, the gain of prestress in the tendon is 0.70 percent, and the maximum center deflection is 0.53 in. down.

A review of the numerical examples (4) indicates that for conditions of moderate temperature variation (25 F) through the depth of prestressed beams, the induced thermal stresses and deflections in the concrete are generally within tolerable design limits.

Stresses in the concrete do not normally exceed the magnitude of about 200 psi in compression and about 100 psi in tension. The induced stress effects in the prestressing tendons range approximately from a 5,000- (3 percent of initial prestress) to about a 8,000-psi (5 percent of initial prestress) loss in stress. The deflections generally lie below 0.04 percent of the span length. Thus, for prestressed concrete beams which are used in bridge structures in moderate climates and are subject only to normal cyclic solar and atmospheric fluctuations, these thermally induced stresses appear to be absorbed by current design procedures and safety factors.

However, note is again made of the high theoretical values of interface shears and moments concentrated at the ends. The extent that these interface stresses are reduced by plasticity, slip, and creep is still an unsettled question. In Guyon's book on prestressed concrete (8), some experimental data are given for deflections of prestressed beams subject to the heat of fire. With the theory presented in this paper, agreement is excellent between theory and test for temperatures up to about 175 F. Since such a limit temperature encompasses normal conditions, it is believed that for those conditions as outlined, the theory set forth is adequate and reliable.

Because of the many complexities involved in the problem of predicting thermal stresses—including creep, slip, and plasticity—no specific recommendations for a simple design specification can be made at this time beyond what has been said. More studies must first be made. However, it is felt that the theories presented in this paper, although complex, can safely be applied, because the unknown effects mentioned will tend to reduce the severity of the induced stresses. Deflections, of course, are an exception, as they will tend to increase.

ACKNOWLEDGMENTS

This paper summarizes the principal findings to date of a long-range program of study sponsored jointly by the Virginia Council of Highway Investigation and Research and the U. S. Bureau of Public Roads. Individual acknowledgment is also made to K. Tatlidil and Y. N. Liu, who as graduate assistants aided in these studies.

REFERENCES

1. Barber, E. S. Calculation of Maximum Pavement Temperatures From Weather Reports. Highway Research Board Bull. 168, pp. 1-8, 1957.
2. Carslaw, H. S., and Jaeger, J. C. Conduction of Heat in Solids. 2nd Ed., pp. 105-106. London, Oxford University Press, 1960.
3. Zuk, W. Thermal and Shrinkage in Composite Beams. Jour. American Concrete Institute, pp. 327-340, Sept. 1961.
4. Liu, Y. N., and Zuk, W. Thermoelastic Effects in Prestressed Flexural Members. Jour. Prestressed Concrete Institute, pp. 64-85, June 1963.
5. Hendry, A. W., and Page, J. K. Thermal Movements and Stresses in Concrete Slabs in Relation to Tropical Conditions. RILEM Symposium on Concrete and R. C. in Hot Countries, Haifa, pp. 11-12, July 1960.
6. Verbundtrager; Strassenbrucken, Richtlinien fur Berechnung und Ausbildung—D1N1078 Blatt 1, Beton Kalender, 1958.
7. Sattler, K. Theorie der Verbundkonstruktionen, Spannbeton Stahltrager in Verbund mit Beton. Berlin, Wilhem Ernst und Sohne, 1959.
8. Guyon, Y. Prestressed Concrete. Pp. 110-112. New York, John Wiley and Sons, 1953.
9. RILEM Symposium on Concrete and R. C. in Hot Countries, Haifa, Part 2, July 1960.
10. Iwamoto, K. On the Continuous Composite Girder. Highway Research Board Bull. 339, pp. 80-90, 1962.
11. The AASHO Road Test, Report 41-1 Bridge Research. Highway Research Board Spec. Rept. 61D, 1962.
12. Hannant, D. J. Thermal Stresses in R. C. Slabs. Magazine of Concrete Research (London), Vol. 14, No. 41, July 1962.
13. Allan, D. W. The Calculation of Temperature Stresses. Concrete and Construction Engr., (London), Vol. 57, No. 9, Sept. 1962.
14. Hirschfeld, K. Der Temperatureinfluss bei der Verbund-Bauweise. Der Bauingenieur (Berlin), Vol. 25, No. 8, pp. 305-306, Aug. 1950.
15. Timoshenko, S., and Goodier. Theory of Elasticity. New York, McGraw-Hill, 1951.
16. Gatewood, B. E. Thermal Stresses. New York, McGraw-Hill, 1957.
17. Steinhardt. Temperaturversuche. Der Bauingenieur (Berlin), Vol. 27, No. 6, pp. 189-190, June 1952.
18. Aleck, B. J. Thermal Stresses in a Rectangular Plate Clamped Along an Edge. Trans. ASME, Vol. 71, pp. 118-122, 1949.
19. Tremmel, E. Temperaturspannungen im Plattenbalken. Osterreichische Bauzeitschrift (Vienna), Vol. 7, No. 1, pp. 1-5, Jan. 1952.
20. Boley and Weiner. Theory of Thermal Stresses. New York, John Wiley and Sons, 1960.
21. Eringer, A. C. Thermal Stresses in Multiple Layer Beam. Proc. 1st Midwestern Conf. of Solid Mechanics, Univ. of Illinois, pp. 69-73, April 1953.
22. Morsch, E. Der Spannbeton Trager. Stuttgart, 1943.
23. Hauelena, E. Brucken in Verbundausweise. Zeitschrift VDI (Dusseldorf), Vol. 90, No. 5, pp. 145-150, 1948.
24. Frohlich, H. Theorie der Stahlverbund-Tragwerke. Der Bauingenieur (Berlin), Vol. 25, No. 3, pp. 80-87, March 1950.
25. Walter, H. Der Einfluss des Schwindens und Kriechens bei Verbundtragern. Beton und Stahlbetonbau (Berlin-Wilmersdorf), Vol. 47, No. 5, pp. 110-115, May 1952.

26. Fritz et al. Discussion. Der Bauingenieur (Berlin), Vol. 25, No. 3, pp. 91-95, March 1950.
27. Tatlidil, K. G. Thermal Stresses in Composite Members Subjected to Temperature Variations Along the Length and in the Depth. C. E. Thesis, Univ. of Virginia, 1962.
28. Liu, Y. N. Thermoelastic Effects in Prestressed Flexural Members. C. E. Thesis, Univ. of Virginia, 1963.
29. England, G. L., and Ross, A. D. Reinforced Concrete Under Thermal Gradients. Magazine of Concrete Research (London), Vol. 14, No. 40, pp. 5-12, March 1962.
30. Zienkiewicz, O. C. Analysis of Visco-Elastic Behavior of Concrete Structures with Particular Reference to Thermal Stresses. Jour. ACI, Vol. 58, No. 4, pp. 383-394, Oct. 1961.
31. Rickenstorf, G. Structural Analysis of Temperature Stresses due to Non-Linear Temperature Distribution in Bars, Slabs, and Plates. Bauplanung-Bautechnik (Berlin), Vol. 13, No. 11, pp. 498-503, Nov. 1949.
32. Kato, M. The Calculation of the Stresses Caused by Shrinkage and Temperature Change in Composite Beams. (In Japanese). Japanese Civil Engineering Techniques, Vol. 14, No. 2, Feb. 1960.
33. Heilig, R. Zur Theorie des Starren Verbunds. Stahlbau, Vol. 22, p. 184, 1953.